HARVARD MEDICAL SCHOOL AND
BRIGHAM AND WOMEN'S HOSPITAL

# Autonomous Renal Calculi Detection, Navigation, and Precise Aiming in Robotic Ureteroscopy and Laser Lithotripsy

**Nicholas Brady** | *Research Intern at the Surgical Navigation and Robotics Lab of Brigham and Women's Hospital and Harvard Medical School, Boston, MA*

## Abstract

The objective of this research was to develop and validate a robotic ureteroscope that could autonomously detect, navigate toward, and precisely aim at renal calculi as part of robotic ureteroscopy and laser lithotripsy. The multi-section robotic ureteroscope used was an advancement of previous work, controlled with a custom 3D Slicer module that was developed during this research. Autonomous guidance was conducted in two stages: gross and fine. During the first stage, gross guidance, the ureteroscope aimed at and advanced toward kidney stones. To identify the stone, hue variations drove a temporally averaged buffer, whose areas of higher concentricity were identified using a K-means grouping approach. Once the ureteroscope was sufficiently near the target stone, primarily determined by the standard deviation of the image brightness, the second stage algorithm, fine guidance, was used for precise aiming. A hue-based region growing algorithm with automatic, lightness-based seed placement was used to segment the stone and precisely aim the ureteroscope at the center. Using 3D-printed kidney stones and multiple kidney phantom calyces, the autonomous detection, navigation, and aiming were evaluated with two metrics: accuracy of the stone centerization, and fine-guidance aiming duration. The results indicated that the robotic ureteroscope demonstrated extremely high accuracy (average error of 0.7 px, approximately 14 μm) and procedurally acceptable aiming duration (10.3 s). Although the aiming duration was statistically significantly greater than the target (two-tailed p-value < 0.001, one-sample t-test), the aiming error was statistically significantly lower than the target (two-tailed p-value < 0.001, one-sample t-test). In conclusion, the developed robotic ureteroscope achieved clinically satisfactory autonomous detection of, navigation toward, and precise aiming at renal calculi.

## Introduction

Treatment of renal calculi, or kidney stones, is typically accomplished by inserting a flexible ureteroscope into the urinary tract, where stones are vaporized via laser lithotripsy [Rosa, et. all 2010]. Insertion into certain calyces, however, is difficult due to poor scope maneuverability, which increases procedure duration and risk of complications [Talari, et. all 2017]. A multi-section Canon continuum robot, developed for transbronchial biopsy [Kato, et. all, 2020], has been optimized for ureteroscopy [Kobayashi, et. al 2023] to improve maneuverability.

There is considerable demand for autonomously aiming robotic catheters for use during surgery. Recently, Boston Children's Hospital demonstrated that an autonomous robotic intracardiac catheter rivals experienced clinician accuracy and speed [Fagogenis, et. all 2019]. It is not yet known, however, if a robotic ureteroscope can autonomously detect, navigate toward, and precisely aim at kidney stones as part of robotic ureteroscopy and laser

lithotripsy. The hypothesis of this research is that a robotic ureteroscope can autonomously detect, navigate toward, and aim at kidney stones with an error of less than 5.5 px and complete aiming in less than 7.0 s.

## Methods

*Experimental Setup*

The experiment was conducted using a Canon Robot (Fig. 1) [Kato, et. all, 2020], a silicone kidney phantom cast from a 3D printed mold [Kobayashi, et. all 2023], and 3D printed kidney stones in a range of sizes (Method-X Printer and ABS-R plastic [Makerbot, New York City, USA]).

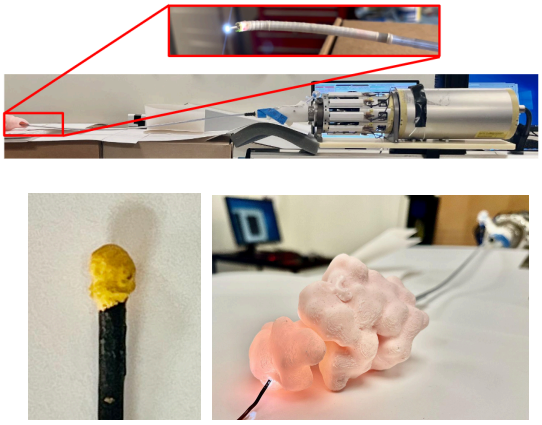

**Fig. 1.**
Overview of the robotic ureteroscope, kidney phantom, and model kidney stone (clockwise). The dual-section tip and embedded camera and light are featured.

*Integration*

The Canon snake robot camera [Kato, et. all, 2020] [Kobayashi, et. all 2023] was controlled with Canon software [Tokuda, et. all 2009]. The video feed was sent through the open-source communication protocol OpenIGTLink [Tokuda, et. all 2009] to a custom-developed 3D Slicer Module used for autonomous guidance. The autonomous guidance software works in two stages: gross guidance, for navigation to the stone, and fine guidance, for precise aiming at the center of the stone.

*Autonomy Stage 1:*

During gross guidance via long-distance detection ( Fig. 2), the image was first filtered with color and contrast adjusted to approximate clinical footage as closely as possible. A normalized hue histogram was then plotted, and peaks were identified within a certain error margin. The image areas of hues within the identified margined peaks were then segmented to identify image regions of like colors. The outlines of each segmentation pertaining to the hues were then overlaid on a blank image, creating a density map of hue variation. A frame buffer was collected and temporally averaged to generate each new frame. Areas of resulting concentricity were then identified using a Hough circle detection algorithm. A K-means algorithm was used to group circles by proximity and identify the coordinates of circle groupings with the highest density, the stone. The coordinates were adjusted and curved for guidance of the robotic ureteroscope during aiming and advancement toward the target. Finally, the standard deviation of the image brightness was monitored for the transition to the Autonomy Stage 2.

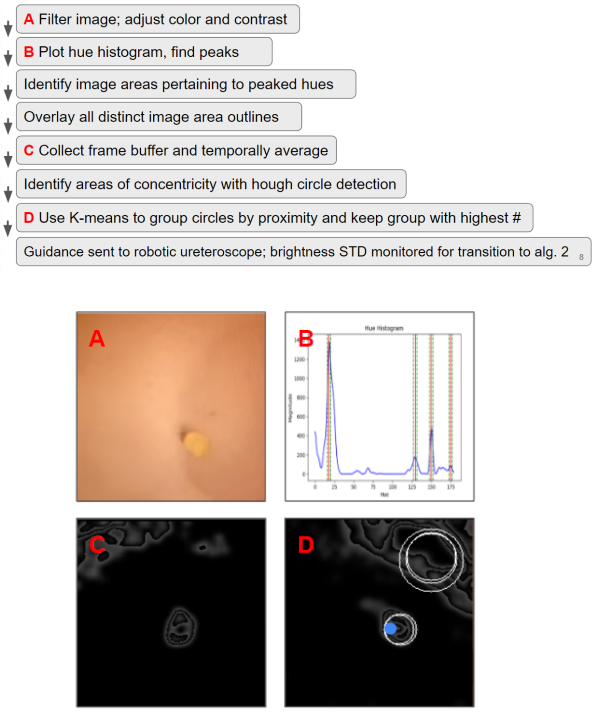


**Fig. 2.**
The first stage in autonomy: gross guidance via long-distance detection. The outline of the detection and guidance algorithm, as well as visual aids for key moments, are presented.

*Autonomy Stage 2:*

During fine guidance, the image was thresholded for brightness and the area with the highest brightness was segmented ( Fig. 3). The center of the thresholded region was identified and designated as the coordinates of the image seed. Using the original image, the color of the region contained by the segmentation was averaged and designated as the seed color. A custom-implemented hue-based region growing algorithm was then initiated from the seed coordinates by testing each neighboring

pixel for similarity to the seed. The coordinates of the center of the seed growing algorithm result were designated as the center of the stone. The coordinates were then adjusted and curved to guide the robotic ureteroscope in precise aiming.

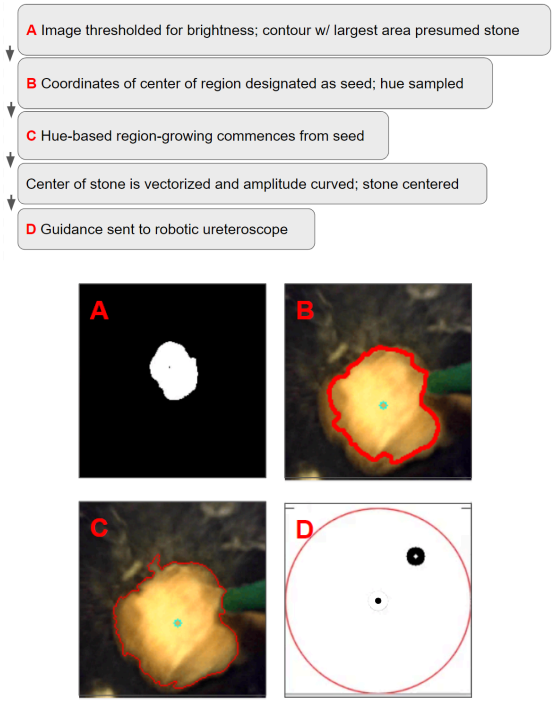


**Fig. 3.**
The second stage in autonomy: fine guidance via close-range segmentation. The outline of the detection and guidance algorithm, as well as visual aids for key moments, are presented.

*Data Collection:*

The autonomous robotic ureteroscope was evaluated using two metrics. Metric 1 was aiming accuracy. After both stages of autonomy, gross and fine guidance, the distance from the center of the image to the center of the stone, in pixels, was measured to determine the aiming accuracy.

The target performance for aiming accuracy was less than 5.5 pixels, approximately 100 µm (Fig. 4). The target was selected because small calipered laser fibers (200-273 µm) are common for ureteroscopic lithotripsy [Kronenberg, et. all 2014] and damage to tissue due to off-target laser pulses may be avoided if the targeting error is below the laser radius.

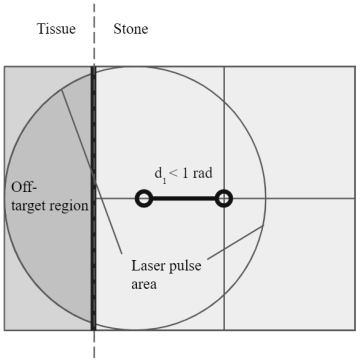


**Fig. 4.**
Borderline between the edge of the kidney stone and tissue with marked laser pulse area and maximum tolerated positional error ($d_1$) to prevent complications.

The second metric was fine-guidance aiming duration, defined as the time taken after the first stage of autonomy, in seconds, for the robot to aim at the center of the stone during fine guidance.

The target performance of the fine-guidance aiming duration was less than 7.0 seconds ( Fig. 5). Stone fragmentation via laser lithotripsy commonly occurs at ~ 5 hz [Talso, et. all 2015]. Assuming a laser diameter of 200 µm [Kronenberg, et. all 2014], the minimum targeting speed to avoid coincision of lasered area is 1 mm/s. Aiming must therefore require fewer than 7.0 s.

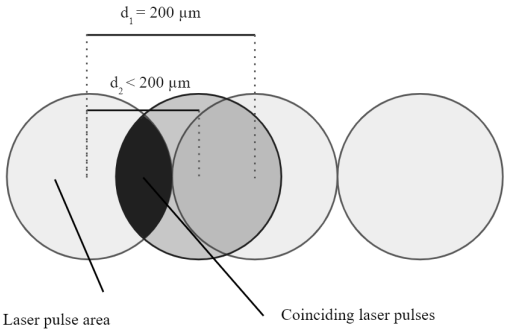


**Fig. 5.**
Consecutive laser pulses with non-overlapping areas and spacing of 200 µm compared against a coinciding laser pulse with a spacing of less than 200 µm, a product of insufficient movement rate.

Ten trials for each metric were conducted in each of five simulated calyces. The stone position was randomized after each trial. The data were evaluated using summary statistics and compared to target values with one-sample t tests.

## Results

The average value of Metric 1 (Fig. 6), aiming accuracy, was 0.7 px (approximately 14 µm), with a standard deviation of 0.4 px, a minimum accuracy of 0.0 px, and a maximum of 1.5 px, relative to the target of 5.5 px. The error was statistically significantly lower than the target of 5.5 pixels (two-tailed p value <0.001, one-sample t test).
The average value of Metric 2 (Fig. 7), fine-guidance aiming duration, was 10.3 seconds, with a standard deviation of 4.4 s, a minimum of 2.6 seconds, and a maximum of 20.5 seconds. The average aiming speed was higher than the target of 7.0 s, although 24% of the data were under the target. The aiming duration was statistically significantly greater than the target of 7 seconds (two-tailed p value < 0.001, one-sample t test).

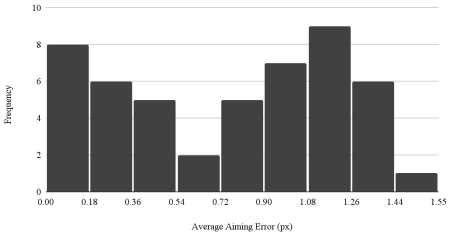


**Fig. 6.**

Frequency of aiming error for robotic ureteroscope.

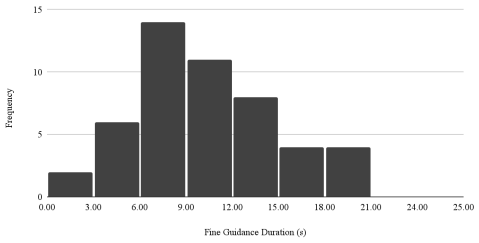


**Fig. 7.**

Frequency of fine-guidance aiming duration for robotic ureteroscope.

## Discussion

It was found that a robotic ureteroscope can autonomously detect, navigate toward, and precisely aim at kidney stones as part of robotic ureteroscopy and laser lithotripsy. The high accuracy found is echoed in literature concerning robotically-assisted ureteroscopy [Talari, et. all 2017]. Further, the reduced operating time exhibited by some of the data is substantiated by separate literature on a robotically-assisted ureteroscope [Zhao, et. all 2021].

Metric 1 (aiming accuracy) drastically outperformed the target, suggesting clinical viability. The bimodal distribution of aiming accuracy (Fig. 6) may be a product of the robot's stepped, forward advancement. The robot advanced forward in 0.5 mm increments, while the stone remained stationary (Fig. 8). Therefore, the distance between the stone and the tip of the ureteroscope varied by less than 0.5 mm. The varying distance from the scope tip and stones produced different hues due to the camera advancing. Thus, two modes of images could occur: the image at ~ 0.75 mm distance (d2) and the image at ~ 0.5 mm distance (d1). The accuracy suffered in the far imaging mode, as the scope was further from the target, and adjustments to the tip position yielded amplified error in centralization accuracy. This issue can be remedied in future work by implementing a more precise linear stage, thus enabling greater control over the linear position of the scope.

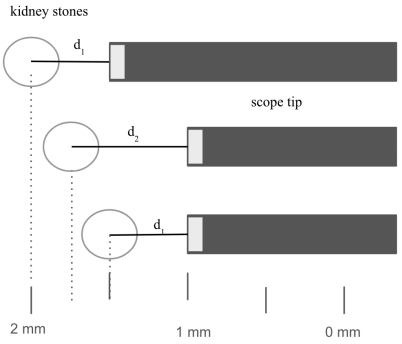


**Fig. 8.**

Variable stone position compared to the stepped, 0.5 mm forward advancement of the robotic ureteroscope tip, thus generating the primary imaging modes $d_1$ (~0.5 mm) and $d_2$ (~0.75 mm).

Metric 2 (fine-guidance aiming duration) exceeded the target but remained clinically satisfactory as the laser pulse rate may be adjusted to suit a slower travel speed. Often the aiming duration was extended by robot overcorrection. The tip was observed to swing past the target, then overcorrect in the opposite direction with overly sufficient speed so as to miss the target again. Future work can improve the guidance duration by adjusting the control vector curve to reduce this oscillation by ensuring that the tip moves at slow enough speeds when near the stone to prevent overshooting the target.

The precise aiming conducted in this study was stone centralization. A "sweeping" motion of the tip, however, is ideal to avoid uncontrolled fragmentation of the stone

and subsequent risk of infection. Automated path generation and premeditated control for this purpose are objectives of future research.

## Conclusion

A robotic ureteroscope that can autonomously detect, navigate toward, and precisely aim at kidney stones as part of robotic ureteroscopy and laser lithotripsy was developed and validated. It was found that the robotic ureteroscope can detect, navigate toward, and aim at kidney stones with an average error of 0.7 px (~14 µm) and an average aiming duration of 10.3 s, which is deemed to be clinically satisfactory.

## Acknowledgments

Professor Nobuhiko Hata, for welcoming me into the lab, assigning the research objective, aiding with the experimental setup and the slideshow presentation that inspired this write-up; Franklin King, for assistance with OpenIGTLink, 3D Slicer, 3D printing, and operating the Snake Robot; and Dr. Daniel Wollin, for requesting the investigation of this research objective.

## References


- Rosa B, Mozer P, Szewczyk J. An algorithm for calculi segmentation on ureteroscopic images. Int J Comput Assist Radiol Surg. 2011 Mar;6(2):237-46. doi: 10.1007/s11548-010-0504-x. Epub 2010 Jun 24. PMID: 20574798.
- Kato, Takahisa & King, Franklin & Takagi, Kiyoshi & Hata, Nobuhiko. (2020). Robotized Catheter With Enhanced Distal Targeting for Peripheral Pulmonary Biopsy. IEEE/ASME Transactions on Mechatronics. PP. 1-1. 10.1109/TMECH.2020.3040314.
- Kobayashi S, Masaki F, King F, Wollin DA, Kibel AS, Hata N. Feasibility of multi-section continuum robotic ureteroscope in the kidney. J Robot Surg. 2023 Aug;17(4):1411-1420. doi: 10.1007/s11701-023-01530-0. Epub 2023 Jan 23. PMID: 36689076.
- Kronenberg P, Traxer O. In vitro fragmentation efficiency of holmium: yttrium-aluminum-garnet (YAG) laser lithotripsy--a comprehensive study encompassing different frequencies, pulse energies, total power levels and laser fibre diameters. BJU Int. 2014 Aug;114(2):261-7. doi: 10.1111/bju.12567. Epub 2014 Apr 16. PMID: 24219145.
- Talso M, Emiliani E, Haddad M, Berthe L, Baghdadi M, Montanari E, Traxer O. Laser Fiber and Flexible Ureterorenoscopy: The Safety Distance Concept. J Endourol. 2016 Dec;30(12):1269-1274. doi: 10.1089/end.2016.0209. PMID: 27733053.
- Tokuda J, Fischer GS, Papademetris X, Yaniv Z, Ibanez L, Cheng P, Liu H, Blevins J, Arata J, Golby AJ, Kapur T, Pieper S, Burdette EC, Fichtinger G, Tempany CM, Hata N. OpenIGTLink: an open network protocol for image-guided therapy environment. Int J Med Robot. 2009 Dec;5(4):423-34. doi: 10.1002/rcs.274. PMID: 19621334; PMCID: PMC2811069
- Talari HF, Monfaredi R, Wilson E, Blum E, Bayne C, Peters C, Zhang A, Cleary K. Robotically assisted ureteroscopy for kidney exploration. Proc SPIE Int Soc Opt Eng. 2017 Feb;10135:1013512. doi: 10.1117/12.2253862. Epub 2017 Mar 3. PMID: 29731536; PMCID: PMC5930009.
- Zhao J, Li J, Cui L, Shi C, Wei G. Design and Performance Investigation of a Robot-Assisted Flexible Ureteroscopy System. Appl Bionics Biomech. 2021 Nov 18;2021:6911202. doi: 10.1155/2021/6911202. PMID: 34840603; PMCID: PMC8616660.
- Fagogenis G, Mencattelli M, Machaidze Z, Rosa B, Price K, Wu F, Weixler V, Saeed M, Mayer JE, Dupont PE. Autonomous Robotic Intracardiac Catheter Navigation Using Haptic Vision. Sci Robot. 2019 Apr 24;4(29):eaaw1977. doi: 10.1126/scirobotics.aaw1977. PMID: 31414071; PMCID: PMC6693882